

■ Electro, Physical & Theoretical Chemistry

Pressure-Induced Amorphization of MOF-5: A First Principles Study

Mustafa Erkartal⁺ and Murat Durandurdu^{+*^[a]}

Amorphous metal-organic frameworks (MOFs) and the amorphization of crystalline MOFs under mechanical stimuli are attracting considerable interest in last few years. However, we still have limited knowledge on their atomic arrangement and the physical origin of crystalline-to-amorphous phase transitions under mechanical stimuli. In this study, ab initio simulations within a generalized gradient approximation are carried out to investigate the high-pressure behavior of MOF-5. Similar to the previous experimental findings, a pressure-

induced amorphization is observed at 2 GPa through the simulations. The phase transformation is an irreversible first order transition and accompanied by around 68% volume collapse. Remarkably, the transition arises from local distortions and, contrary to previous suggestions, does not involve any bond breaking and formation. Additionally, a drastic band gap closure is perceived for the amorphous state. This study has gone some way towards enhancing our understanding of pressure-induced amorphization in MOFs.

Introduction

Crystalline metal-organic frameworks (MOFs) are built by the organic linkers and inorganic metal/metal clusters nodes via coordination bonds.^[1] The formed 2D or 3D network solids have large pores without curtain-like walls^[2] that are very useful for gas storage,^[3] gas separation,^[4] catalyst,^[5] electrochemical,^[6] and biomedical applications.^[7] Within the next few years, MOFs are likely to become one of important engineering materials in mentioned areas. However, a few publications that discuss the behaviors of MOFs under mechanical stimuli are available in the literatures.

Defining structural transitions between crystalline and amorphous phases is one of the most fundamental problems in Materials Science. Many crystalline porous materials, for instance zeolites, can be amorphized under relatively low pressures, a phenomenon so-called pressure-induced amorphization (PIA).^[8] When impulses or external pressures are applied to the porous materials, they can lead to several mechanical processes, such as compaction or compression of the materials. As a result of these mechanical processes, the pores inside the MOFs can collapse and the crystal framework may effortlessly transform into an amorphous structure.^[9]

Amorphous MOFs (α -MOFs), considered as a revolutionary idea, are formed by the linkage of metal nodes with organic ligands as in the case of their crystal counterparts, but they do not have a long-range order.^[10] To date, pressure,^[11] ball milling,^[12] heating,^[13] electrical-discharge^[14] have been used to produce α -MOFs from crystalline frameworks. Various applica-

tions - such as drug delivery,^[15] storage of nuclear waste^[6b,16] - which are based on collapsing of porous host MOF structures around guest species have been proposed for α -MOFs. Additionally, the pressure-induced bond breakage can offer a promising application of MOFs as a mechanical energy absorber for shock compressions.^[17] However, there has been little discussion on the atomic-scale mechanism of amorphization in MOFs to date.

Amongst numerous MOFs, MOF-5, first synthesized by Yaghi and co-workers,^[18] is one of the most well-known materials. It has Zn_4O clusters coordinated by benzene-1,4,-dicarboxylic acid (BDC) linkers to form a cubic 3D framework.^[19] Up to now, considerable efforts have been devoted to investigate its gas storage properties both experimentally and theoretically due to its high specific surface area, 4700 m²/g.^[20] In recent years there have been growing theoretical interests to probe its electronic,^[21] optical,^[22] mechanical^[23] and spectroscopic^[22b,23c] properties. Furthermore, there have been few new studies that discuss the potential usage of MOF-5 as quantum dots,^[24] photocatalysts,^[25] semiconductor materials,^[26] supercapacitor components,^[27] and fuel cell electrodes.^[28] To the best of our knowledge, there are two reports, showing the mechanical amorphization of MOF-5, in the literature. In the first study, Hu et al. experimentally revealed a pressure-induced amorphization in a polycrystalline MOF-5 sample at room temperature and 3.5 MPa. They pointed out that the destruction of carboxylate groups could be a main reason behind the amorphization.^[11a] In the second one, Moggach et al.^[29] showed the complete amorphization of a single crystal MOF-5 sample above 3.2 GPa in a diamond anvil cell (DAC) experiment using diethyl formamide (DEF) as a pressure transmitting medium. The authors underlined that the amorphization of framework might be related to Zn-O bonds.^[29]

In this report, inspired by both previous works, we investigated the PIA in MOF-5 by using a constant pressure ab initio technique to have an atomistic level description of this

[a] M. Erkartal,⁺ Prof. M. Durandurdu⁺
Abdullah Gül University, Materials Science & Nanotechnology Engineering, Kayseri, Turkey
E-mail: murat.durandurdu@agu.edu.tr

[⁺] The manuscript was written through contributions of all authors. All authors have given approval to the final version of the manuscript.

phase transition. During the simulations, the crystalline MOF-5 phase was subjected to a gradually increased hydrostatic pressure, and the collapsing of the pores was observed at 2 GPa, which resulted in an irreversible first-order phase transition in the framework. Further, we performed the Bader charge analysis to explore the charge transfers among atoms during this transition and investigated the electronic structure of both crystalline and amorphous states. Our calculations show that amorphization is due to the local structural distortions without any breaking bonds in the framework, and a charge transfer occurs between Zr–O and C–H. We believe that this study has gone some way towards enhancing our understanding of crystalline-to-amorphous phase transitions in MOFs.

Results and Discussion

The porous framework structure of MOF-5 formed by linking Zn_4O nodes with BDC ligands has a cubic $Fm\bar{3}m$ symmetry (no. 225) with the lattice parameter of $a_0 = 25.866 \text{ \AA}$. Prior to the application of pressure, experimentally obtained X-ray diffraction structure^[19] was optimized via a CG method with 0.01 eV/Å force tolerance at zero pressure. The equilibrium lattice parameter and structural data obtained are in good agreement with the experimentally elucidated structure of MOF-5 as seen from Table 1. Yet, a small difference between the experimental

Table 1. Optimized structural parameters for MOF-5				
Property	PBE-GGA	Exp. ^[19]	PBE-GGA ^[22b]	LDA ^[23c]
Crystal System	Cubic	Cubic	Cubic	Cubic
Space Group	$Fm\bar{3}m$	$Fm\bar{3}m$	$Fm\bar{3}m$	$Fm\bar{3}m$
a_0 (Å)	26.236	25.885	26.044	25.888
V_0 (Å ³)	18060	17344	17665	17350
ρ (g/cm ³)	0.57	0.59	-	0.589
Atom Type	Atomic Positions (x,y,z)		Atomic Positions (x,y,z) ^[19]	
Zn ₁ (32 f)	(0.2937, 0.2937, 0.2937)		(0.2935, 0.2935, 0.2935)	
O ₁ (8 c)	(0.2500, 0.2500, 0.2500)		(0.2500, 0.2500, 0.2500)	
O ₂ (96 k)	(0.2187, 0.7810, 0.3668)		(0.2194, 0.7806, 0.3661)	
C ₁ (48 g)	(0.2500, 0.8853, 0.2500)		(0.2500, 0.8885, 0.2500)	
C ₂ (48 g)	(0.2500, 0.9467, 0.2500)		(0.2500, 0.9461, 0.2500)	
C ₃ (96 k)	(0.7170, 0.2826, 0.4734)		(0.7175, 0.2825, 0.4734)	
H ₃ (96 k)	(0.6916, 0.3085, 0.4528)		(0.6956, 0.3044, 0.4552)	

and calculated lattice parameter originates from the fact that the GGA-PBE approach generally overestimates the lattice parameters.^[30]

After the relaxation process, the gradually increased hydrostatic pressure was applied to the equilibrated structure and the change in the volume and structure was monitored. The Figure 1 presents the pressure dependence of conventional cell volume and the evolution of a subunit consisting of BDC and Zn linkage nodes. A sharp decrease in the volume (68%) indicates a first-order phase transition at 2 GPa. Beyond this pressure, there is an insignificant change in the volume. Upon decompression from 4 GPa, the structure only recovers a small

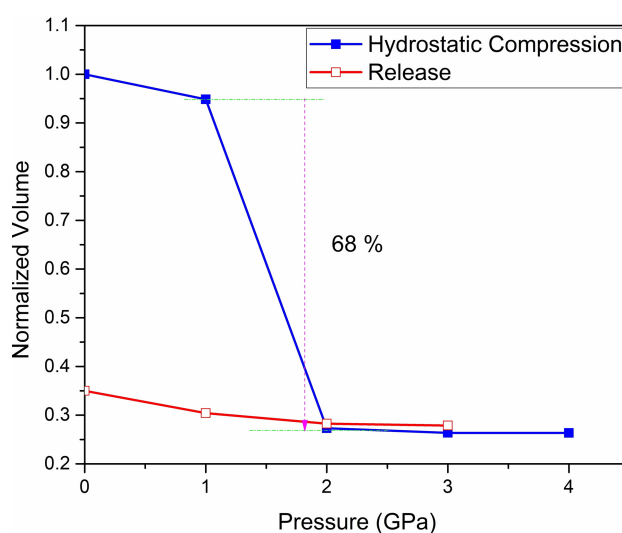


Figure 1. Pressure dependence of conventional cell volume.

percentage (~6%) of its original volume, indicating the irreversible nature of this transition.

In order to identify the structure at this pressure and compare it with the MOF-5 crystal at ambient pressure, we first probe their total and partial pair distribution functions (PDFs), which can provide detailed information on their short-range order (SRO). Total and partial PDFs for both structures are given Figure 2. The results disclose quite different PDFs for them as expected, specifically beyond 4 Å. The PDFs of MOF-5 show long-range correlations (have a pattern with discontinuous and sharp peaks along the given range) though PDFs of the structure at 2 GPa contain relatively less intense peaks up to 4 Å and present typical characteristics of an amorphous state such that it has a well-defined short-range order and the lack of long-range correlations. This observation suggests the occurrence of a pressure-induced amorphization at this pressure in the simulation.

Our coordination number analysis using the first minimum of the PDFs suggests that the coordination number of each species does not change during the phase transformation. This finding does not corroborate the experimental findings and suggestions. Obviously, the local structural distortions, especially in the vicinity of Zn_4O nodes, diminish the long-range order, namely its crystallinity (Figure 3).^[8b,10a] Our structural analysis shows that a new reconstruction mechanism without any bond breaking in the framework is possible due to the free rotation ability of the C–C single bonds on the both sides of the ligands.

The determined bond lengths from the chosen subunit depicted in Figure 4 for MOF-5 and amorphous MOF-5 along with the experimental values are listed in Table 2. According to the results obtained, the bond lengths slightly change during the phase transition. For example, for the crystalline MOF-5 at zero pressure, the C₃–O₁, O₁–Zn, O₂–Zn bond lengths are 1.284, 1.988, and 1.988 Å, respectively. For the amorphous form at 2 GPa, the C₃–O₁, O₁–Zn, O₂–Zn bond lengths alter to 1.279,

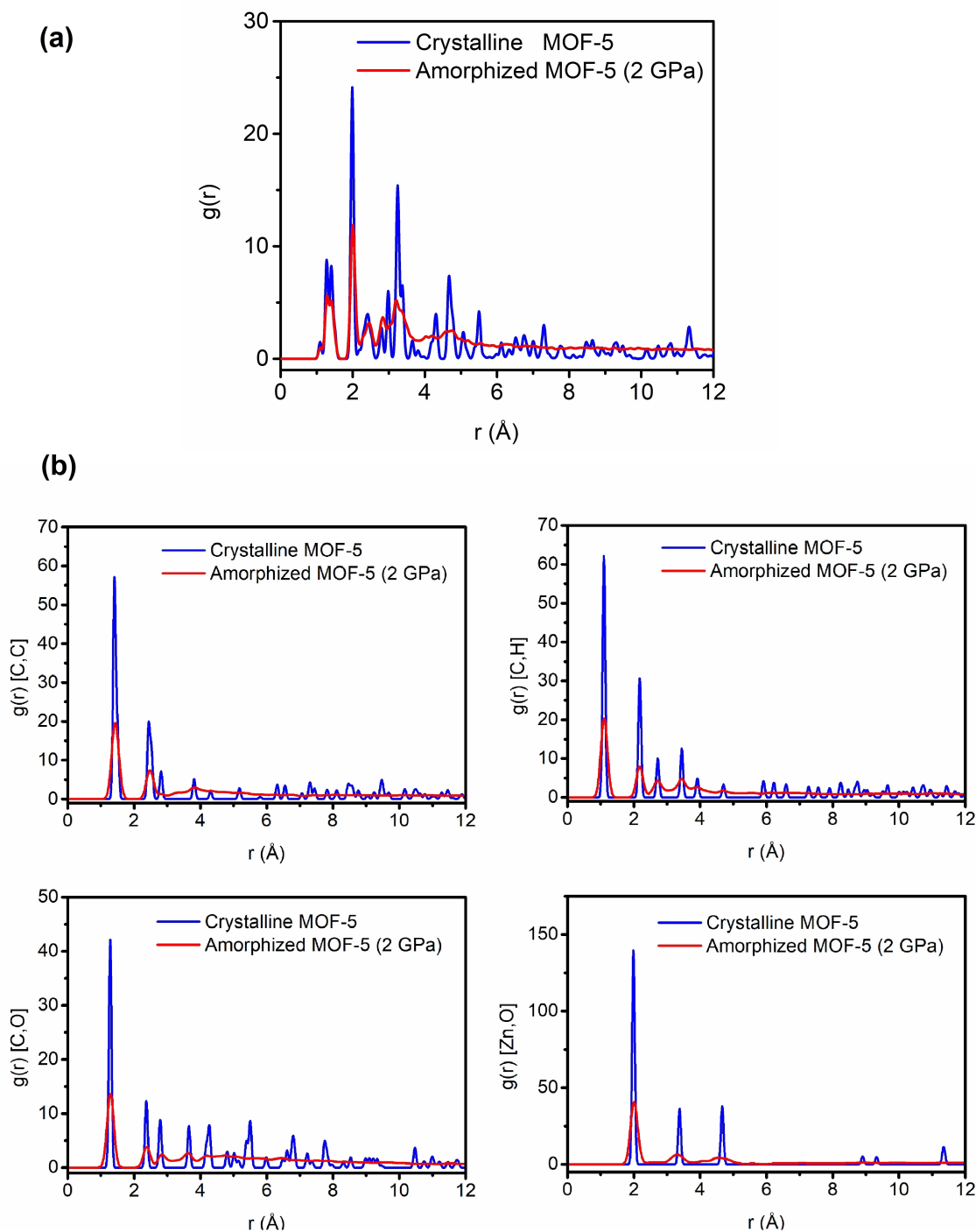


Figure 2. (a) Total and (b) partial pair-distribution functions (PDFs) for the crystalline MOF-5 phase and its amorphized form at 2 GPa.

2.008 and 1.967 Å, correspondingly. Furthermore, in order to investigate the structural deformation in details, we plot the bond angle distribution functions of both structures. From the histograms as shown in Figure 5, we can see that the pressure causes significant alterations on the bond angles. For instance, the O–Zn–O angles are at 106° and 110° for MOF-5 and range from 89° to 140° for the amorphous state. Similarly, while Zn–

O–Zn angle is located at 131° for the crystalline structure, it ranges from 85° to 130° in the amorphous form.

The calculated total electronic density of states (TDOS) and partial density of states (PDOS) at different pressures are shown in Figure 6. The estimated GGA band gap value for MOF-5 is 2.5 eV, indicating that this structure has a semiconducting property. As might have been expected, this value is much

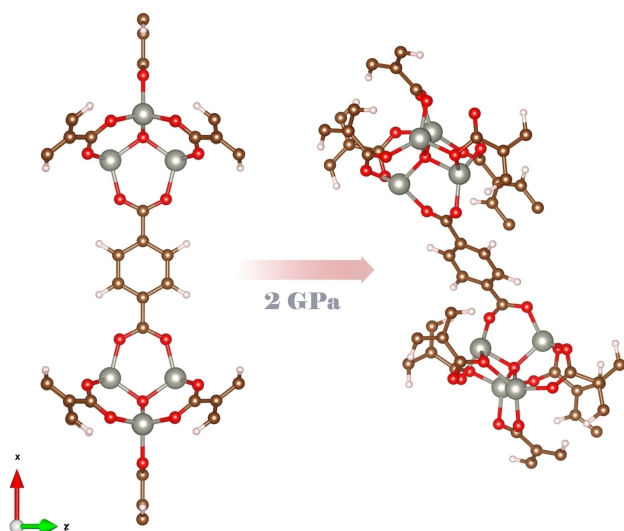


Figure 3. Structural evolution of extracted subunit from conventional cell.

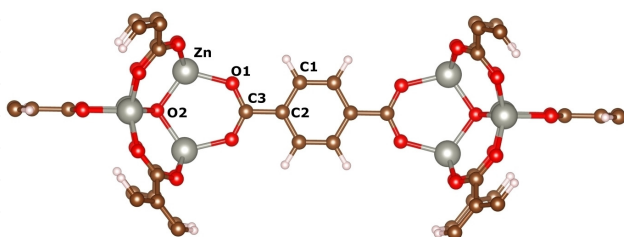


Figure 4. Extracted subunit from the conventional cell of MOF-5. Zinc, oxygen, carbon, and hydrogen are presented in grey, red, brown and white, respectively.

Table 2. Calculated bond lengths for optimized structure and α -MOF-5			
Bond	MOF-5 (GGA-PBE) (Å)	α -MOF-5 (2 GPa) (Å)	Exp. MOF-5 (Å) ^[19]
C ₁ -C ₂	1.412	1.407	1.383
C ₂ -C ₃	1.498	1.486	1.500
C ₃ -O ₁	1.284	1.279	1.262
O ₁ -Zn	1.988	2.008	1.940
O ₂ -Zn	1.988	1.967	1.938
C-H	1.10	1.10	0.97

lower than experimentally obtained band gap energy of 3.4–4.0 eV for MOF-5^[31] since DFT-GGA methods generally yield a lower band gap due to the ground-state formalism of DFT.^[32] The overall electronic properties of MOF-5 are governed by both inorganic Zn₄O nodes and organic BDC linker. In this context, the metallic Zn₄O nodes give the structure a wide band gap property.^[31b] The delocalized electrons in the BDC may seem to improve the conductivity of the structure because the conduction is interrupted at insulating Zn₄O nodes.^[32c] PDOSs provide further perspective how both components contribute the formation of valance and conduction bands. It is apparent from Figure 6 that the bottom of the conduction band is determined by the unoccupied s and p states of the

C, O and Zn atoms, while the top of the valance band is predominantly formed by the hybridization of the 2p-states of C and O with Zn-3d states.

Also as can be clearly seen from the graph, for the structure at 1 GPa, no significant difference was found in the electronic structures. This might be predictable because there is no notable structural change in the framework at this pressure and its crystallinity is preserved. On the other hand, accompanied by the phase transformation, interesting and remarkable changes are observed in the electronic structure. The band gap drops to 1.5 eV at 2 GPa.

The Bader charge analysis is an unbiased method to determine changes in atomic charges and volumes. In this technique, a complex chemical system –such as a molecule– can be partitioned into single atomic (Bader) volumes. Each Bader volume has a single charge density maximum. Also, these volumes are separated from each other by surfaces where the charge density is a minimum normal to the surface. Thus, there is only one Bader volume for each atom and one charge density maximum at each atomic center. So, the Bader charge analysis is a well-defined, precise and useful method, and also more robust than wavefunction-based population analysis (for example, Mulliken population analysis).^[33] Furthermore, the Bader charge analysis can be used for the investigation of phase-transitions.^[34] Here, the Bader charge analysis was employed in order to explore roles of atomic charges and volumes in the crystalline-to-amorphous phase transition in MOF-5. The results are summarized in Figure 7a–7b. Both the Bader charge and volume plots are parallel to the pressure-volume curve of MOF-5. At ambient pressure, due to large electronegativity difference between Zn ($\chi=1.65$) – O ($\chi=3.44$) and C ($\chi=2.55$) – O ($\chi=3.44$) atom pairs, each O₁ and O₂ atoms gain ~ 1.08 and $\sim 1.25e$ from each C₃ and Zn atoms, respectively. The calculated the Bader volume for O₁ atom (113 Å³) and O₂ atom (102 Å³) are about much higher than C₃ atom (42 Å³) and Zn atom (81 Å³), and this also confirms the charge transfers between referred atoms. During the phase transition at 1–2 GPa, a significant charge transfer was observed between Zn-O₁, O₁-C₃ and terminal H atoms. At this pressure range, the Bader charge results show that about 0.13e moved from Zn and O₁ atoms to C₃ and H* atoms. Beyond the phase transition range, at 2–4 GPa, there is no significant charge transfer between the constituents' atoms. Moreover, the Bader analysis of individual atoms in the simulated cell shows that in the crystalline phase the Bader charges and volumes differences for the same atoms are very small, while in the amorphous phase there are significant fluctuations in charges and volumes. (Figure S1–S14) This is probably due the lack of a long-range order but almost the same short-range order around the same kind atoms.

In general, the analysis of the coordination number, bond lengths, and angles expose that the crystalline-to-amorphous phase transition is a result of local distortions i.e. bond bending in the framework and does not involve any new bond formation or breaking. It would appear that the structural changes mainly act on the Zn₄O nodes and coordination sites. These findings are in contradiction with Hu et al.'s report,

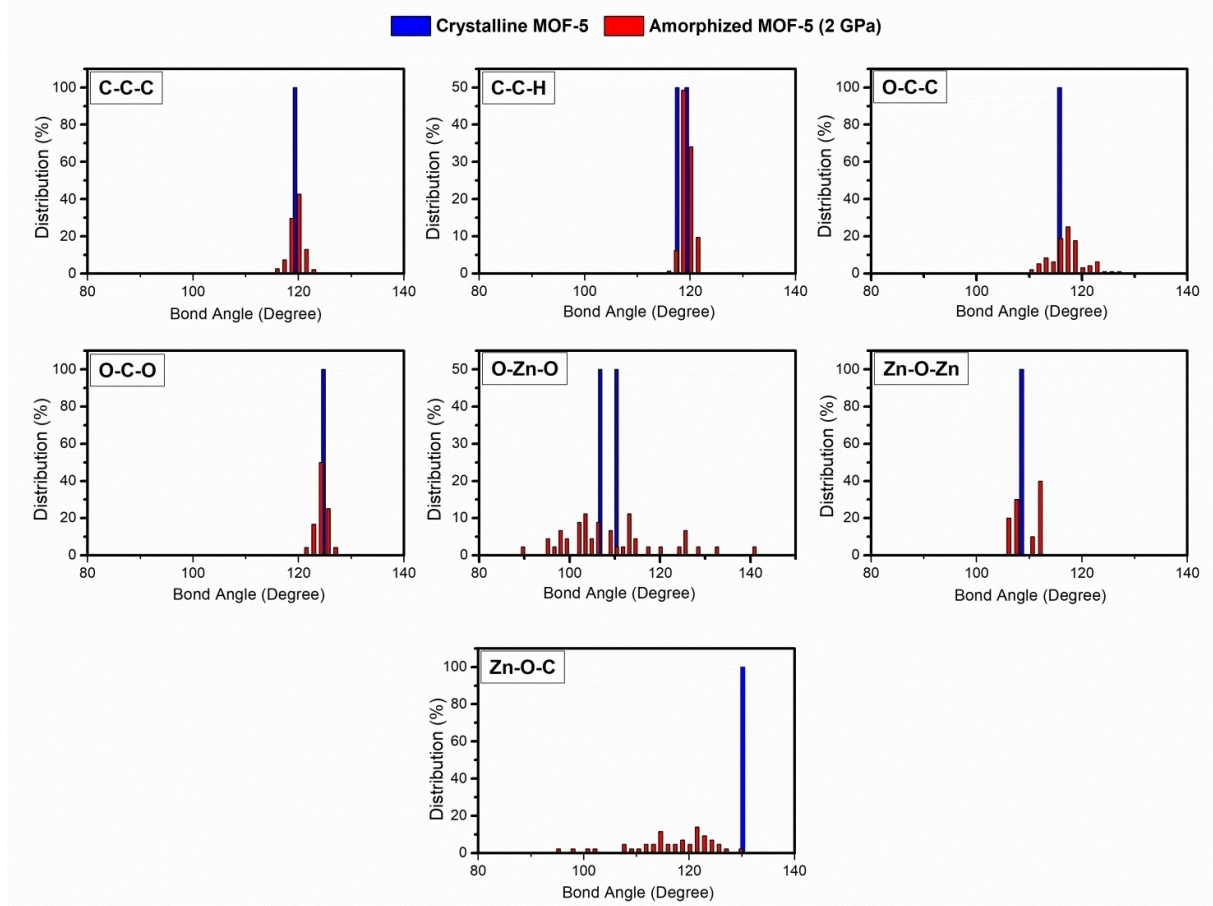


Figure 5. Bond angles distributions for the crystalline MOF-5 and α -MOF-5 phases.

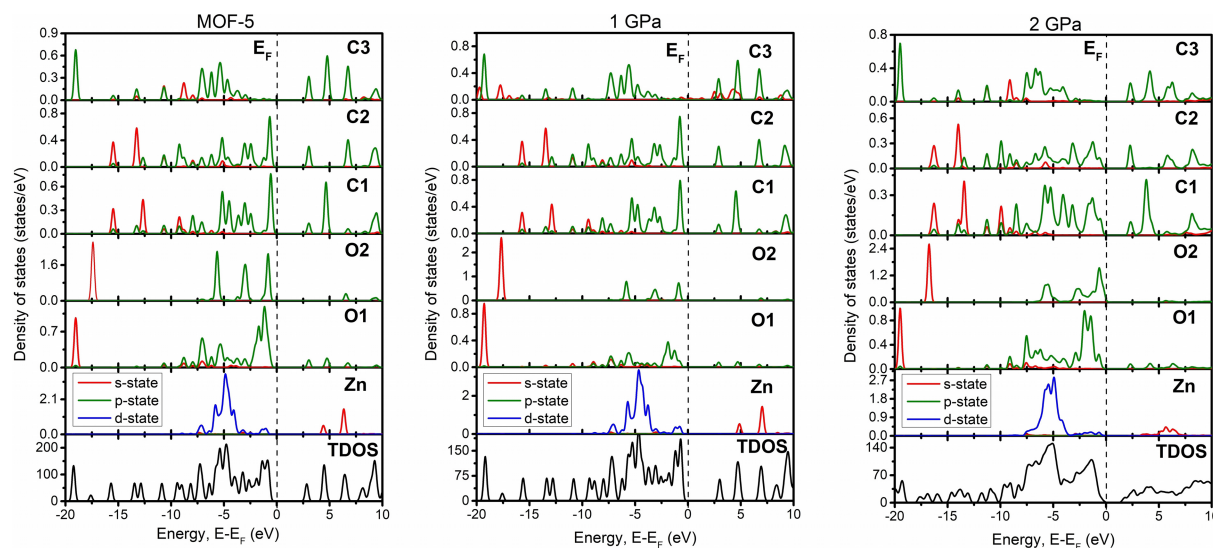
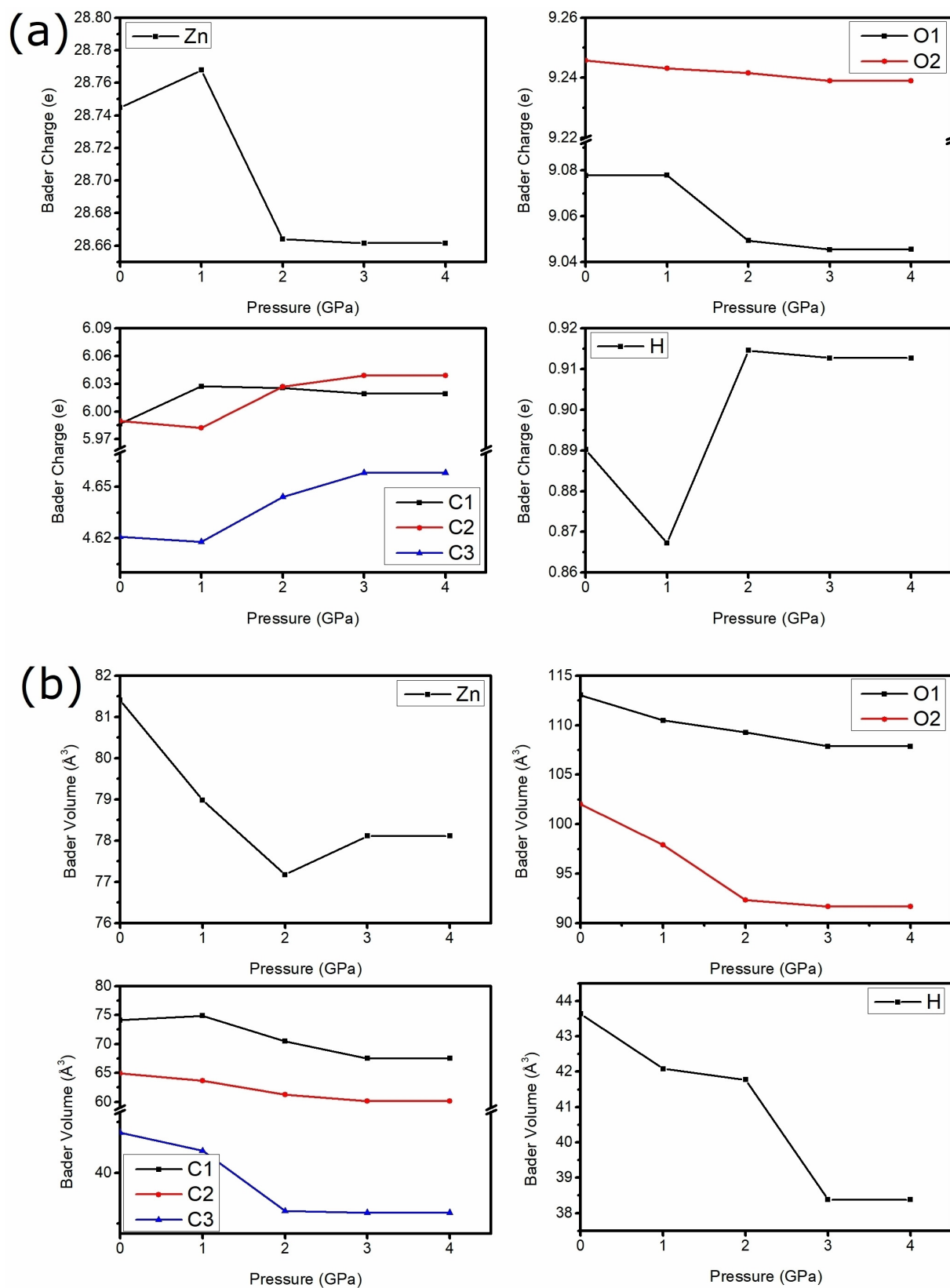


Figure 6. Calculated total density of states (TDOS) and partial density of states (PDOS) for MOF-5, the structure at 1 GPa and α -MOF-5.

where they claimed that pressure-induced amorphization occurs via the destroying some carboxylate groups. Additionally, their amorphization pressure (3.5 MPa) is significantly lower

than what we found in the simulation (2 GPa). The difference between the simulation conditions and experimental conditions is probably responsible for this inconsistency. In our study,



there are no factors, such as surface effects due to the use of periodic boundary conditions and structural defects that can significantly influence phase transitions in the simulated framework. On the other hand, Hu et al.^[11a] reported the amorphization of a polycrystalline pellet MOF-5 sample, including crystal-crystal interaction, surface and boundary defects, and uniaxial nature of applied pressure. In a different work, Moggach et al. testified the complete amorphization of a single crystal MOF-5 sample at 3.2 GPa in a DAC experiment in which the diethyl formamide (DEF) was used as a pressure-transmitting medium (PTM). They pointed out that the squeezing of PTM molecules into pores leads to delaying the onset of amorphization of framework. This feature could well be responsible for the difference in amorphization pressures between the simulation and experiment. Moggach et al.^[29] also highlighted that the amorphization of MOF-5 was governed by change in Zn–O bonds. According to our bond length calculations, both Zn–O1 bonds (to the carboxyl oxygen atom) and Zn–O2 bonds (to the μ^4 -oxygen atom) moderately change during the phase transition. The Bader charge analysis further shows the charge transfers between Zn, O and C (to the carboxyl carbon atom) atoms, and provides insight about the alterations in these bond lengths through the crystalline-to-amorphous phase transition. Importantly, the amorphization of framework leads to a drastic narrowing in band gap energy. Therefore, pressurizing or pressure-induced amorphization can be used in band-gap engineering of MOFs.

In the literature, pressure-induced transitions (PIT) of MOFs are commonly referred as adsorption-induced transitions (AIPs). Although AIPs are very useful to describe the transitions in gas adsorption applications, it is insufficient to directly determine the mechanical behavior of frameworks. Namely, once the pores of the MOF are filled with adsorbate molecules, the framework turns into more resilient structure, which is considerably different than porous structure. Furthermore, the adsorbent-adsorbate interactions may affect the phase transition characteristics. Similarly, the DAC experiments in the existence of the PTM are also inadequate to directly determine the mechanical properties of MOFs due to the strong framework-PTM interactions. The *in situ* TEM compression test proposed by Suslick^[9] seems to be a reliable approach to determining the mechanical properties and amorphization pressure of single crystal MOFs. However, due to the requirement of equipment infrastructures, it is unlikely that these experiments are widely available for now. On the other hand, ab initio simulations allow the modeling of framework under desired pressure (isotropic, uniaxial, etc.) and taking into account quantum mechanical phenomena (charge transfer, bonding, etc.), as well as it is easily accessible and provides reproducible simulations.

Conclusion

In conclusion, this study represents an investigation of pressure-induced amorphization in MOF-5 by using an ab initio technique. We have successfully observed an irreversible crystal-to-amorphous phase transition at 2 GPa and propose

that the origin of phase transition is due to the local distortions through the framework, and does not involve any bond breaking and/or formation. Furthermore, the results show that the electronic properties of the crystalline MOF-5 phase are considerably different than the amorphous phase. We believe that our results may improve the knowledge about pressure-induced amorphization in MOFs.

Supporting Information Summary

Supporting information includes the calculation details, the Bader charges and volumes of individual atoms at all pressures, Figures S1–S14, and Table S1–S2 and also atomic coordinates for simulated systems.

The Bader charge analysis in SIESTA code, an artificial core of 1 electron is initially added for hydrogen. Therefore, at the end of analysis, we subtracted the added artificial core electron from calculated the Bader charge of hydrogen atom.

X = Electronegativity

Acknowledgement

This work was supported by Abdullah Gül University Scientific Research Projects (BAP) under contract number FBA-2017-86. The calculation were partially run on TUBITAK ULAKBİLİM, High Performance and Grid Computing Center (TRUBA resources)

Conflict of Interest

The authors declare no conflict of interest.

Keywords: ab-initio · amorphous-MOF · metal-organic frameworks (MOF) · pressure-induced amorphization (PIA)

- [1] G. Ferey, *Chem Soc Rev* **2008**, *37*, 191–214.
- [2] E. A. Kapustin, S. Lee, A. S. Alshammari, O. M. Yaghi, *Acs Central Sci* **2017**, *3*, 662–667.
- [3] a) D. Alezi, Y. Belmabkhout, M. Suyetin, P. M. Bhatt, L. J. Weselinski, V. Solovyeva, K. Adil, I. Spanopoulos, P. N. Trikalitis, A. H. Emwas, M. Eddaoudi, *J Am Chem Soc* **2015**, *137*, 13308–13318; b) O. K. Farha, A. O. Yazaydin, I. Eryazici, C. D. Malliakas, B. G. Hauser, M. G. Kanatzidis, S. T. Nguyen, R. Q. Snurr, J. T. Hupp, *Nat Chem* **2010**, *2*, 944–948; c) M. Hirscher, *Angew Chem Int Edit* **2011**, *50*, 581–582; d) H. Furukawa, N. Ko, Y. B. Go, N. Aratani, S. B. Choi, E. Choi, A. O. Yazaydin, R. Q. Snurr, M. O’Keeffe, J. Kim, O. M. Yaghi, *Science* **2010**, *329*, 424–428; e) M. Erkartal, U. Sen, *Acs Appl Mater Inter* **2018**, *10*, 787–795; f) M. Erkartal, U. Erkilic, B. Tam, H. Usta, O. Yazaydin, J. T. Hupp, O. K. Farha, U. Sen, *Chem Commun* **2017**, *53*, 2028–2031.
- [4] a) T. Rodenas, I. Luz, G. Prieto, B. Seoane, H. Miro, A. Corma, F. Kapteijn, F. X. L. I. Xamena, J. Gascon, *Nat Mater* **2015**, *14*, 48–55; b) Z. X. Kang, L. L. Fan, D. F. Sun, *J Mater Chem A* **2017**, *5*, 10073–10091; c) R. Banerjee, A. Phan, B. Wang, C. Knobler, H. Furukawa, M. O’Keeffe, O. M. Yaghi, *Science* **2008**, *319*, 939–943.
- [5] a) J. Lee, O. K. Farha, J. Roberts, K. A. Scheidt, S. T. Nguyen, J. T. Hupp, *Chem Soc Rev* **2009**, *38*, 1450–1459; b) J. Gascon, A. Corma, F. Kapteijn, F. X. L. I. Xamena, *Acs Catal* **2014**, *4*, 361–378.
- [6] a) U. Sen, M. Erkartal, C. W. Kung, V. Ramani, J. T. Hupp, O. K. Farha, *Acs Appl Mater Inter* **2016**, *8*, 23015–23021; b) D. Sheberla, J. C. Bachman, J. S. Elias, C. J. Sun, Y. Shao-Horn, M. Dinca, *Nat Mater* **2017**, *16*, 220–224; c) M. G. Campbell, M. Dinca, *Sensors* **2017**, *17*, 1108; d) M. Erkartal, H. Usta, M. Citir, U. Sen, *J Membrane Sci* **2016**, *499*, 156–163; e) H. B.

- Aiyappa, J. Thote, D. B. Shinde, R. Banerjee, S. Kurungot, *Chem Mater* **2016**, *28*, 4375–4379.
- [7] a) R. Liu, T. Yu, Z. Shi, Z. Y. Wang, *Int J Nanomed* **2016**, *11*; b) S. Keskin, S. Kizilel, *Ind Eng Chem Res* **2011**, *50*, 1799–1812.
- [8] a) I. Peral, J. Iniguez, *Phys Rev Lett* **2006**, *97*, 225502; b) K. W. Chapman, D. F. Sava, G. J. Halder, P. J. Chupas, T. M. Nenoff, *J Am Chem Soc* **2011**, *133*, 18583–18585.
- [9] Z. Su, Y. R. Miao, S. M. Mao, G. H. Zhang, S. Dillon, J. T. Miller, K. S. Suslick, *J Am Chem Soc* **2015**, *137*, 1750–1753.
- [10] a) T. D. Bennett, A. L. Goodwin, M. T. Dove, D. A. Keen, M. G. Tucker, E. R. Barney, A. K. Soper, E. G. Bithell, J. C. Tan, A. K. Cheetham, *Phys Rev Lett* **2010**, *104*, 115503; b) H. Ohtsu, T. D. Bennett, T. Kojima, D. A. Keen, Y. Niwa, M. Kawano, *Chem Commun* **2017**, *53*, 7060–7063; c) R. Gaillac, P. Pullumbi, K. A. Beyer, K. W. Chapman, D. A. Keen, T. D. Bennett, F. X. Coudert, *Nat Mater* **2017**, *16*, 1149–1154; d) T. D. Bennett, T. K. Todorova, E. F. Baxter, D. G. Reid, C. Gervais, B. Bueken, B. Van de Voorde, D. De Vos, D. A. Keen, C. Mellot-Draznieks, *Phys Chem Chem Phys* **2016**, *18*, 2192–2201; e) P. Zhao, T. D. Bennett, N. P. M. Casati, G. I. Lampronti, S. A. Moggach, S. A. T. Redfern, *Dalton T* **2015**, *44*, 4498–4503; f) T. D. Bennett, A. K. Cheetham, *Accounts Chem Res* **2014**, *47*, 1555–1562.
- [11] a) Y. H. Hu, L. Zhang, *Phys Rev B* **2010**, *81*; b) K. W. Chapman, G. J. Halder, P. J. Chupas, *J Am Chem Soc* **2009**, *131*, 17546–17547.
- [12] a) S. Cao, T. D. Bennett, D. A. Keen, A. L. Goodwin, A. K. Cheetham, *Chem Commun* **2012**, *48*, 7805–7807; b) T. D. Bennett, S. Cao, J. C. Tan, D. A. Keen, E. G. Bithell, P. J. Beldon, T. Friscic, A. K. Cheetham, *J Am Chem Soc* **2011**, *133*, 14546–14549.
- [13] a) M. R. Ryder, T. D. Bennett, C. S. Kelley, M. D. Frogley, G. Cinque, J. C. Tan, *Chem Commun* **2017**, *53*, 7041–7044; b) T. D. Bennett, D. A. Keen, J. C. Tan, E. R. Barney, A. L. Goodwin, A. K. Cheetham, *Angew Chem Int Edit* **2011**, *50*, 3067–3071 (*Angew Chem* **2011**, *123*, 3123–3127).
- [14] Y. Zhou, C. J. Liu, *Plasma Chem Plasma P* **2011**, *31*, 499–506.
- [15] a) C. Orellana-Tavra, E. F. Baxter, T. Tian, T. D. Bennett, N. K. H. Slater, A. K. Cheetham, D. Fairen-Jimenez, *Chem Commun* **2015**, *51*, 13878–13881; b) C. Orellana-Tavra, R. J. Marshall, E. F. Baxter, I. A. Lazaro, A. Tao, A. K. Cheetham, R. S. Forgan, D. Fairen-Jimenez, *J Mater Chem B* **2016**, *4*, 7697–7707.
- [16] a) B. Y. Li, X. L. Dong, H. Wang, D. X. Ma, K. Tan, Z. Shi, Y. J. Chabal, Y. Han, J. Li, *Faraday Discuss* **2017**, *201*, 47–61; b) T. D. Bennett, P. J. Saines, D. A. Keen, J. C. Tan, A. K. Cheetham, *Chem-Eur J* **2013**, *19*, 7049–7055.
- [17] Y.-R. M. Zhi Su, Guanghui Zhang, Jeffrey T. Miller, Kenneth S. Suslick, *Chemical Science* **2017**, *8*, 8004–8011.
- [18] N. L. Rosi, J. Eckert, M. Eddaoudi, D. T. Vodak, J. Kim, M. O’Keeffe, O. M. Yaghi, *Science* **2003**, *300*, 1127–1129.
- [19] H. Li, M. Eddaoudi, M. O’Keeffe, O. M. Yaghi, *Nature* **1999**, *402*, 276–279.
- [20] S. S. Kaye, A. Dailly, O. M. Yaghi, J. R. Long, *J Am Chem Soc* **2007**, *129*, 14176–14177.
- [21] a) R. Warmbier, A. Quandt, G. Seifert, *J Phys Chem C* **2014**, *118*, 11799–11805; b) L. M. Yang, G. Y. Fang, J. Ma, E. Ganz, S. S. Han, *Cryst Growth Des* **2014**, *14*, 2532–2541; c) B. Civalleri, F. Napoli, Y. Noel, C. Roetti, R. Dovesi, *Crystengcomm* **2006**, *8*, 364–371.
- [22] a) L. M. Yang, G. Y. Fang, J. Ma, R. Pushpa, E. Ganz, *Phys Chem Chem Phys* **2016**, *18*, 32319–32330; b) L. M. Yang, P. Vajeeston, P. Ravindran, H. Fjellvag, M. Tilset, *Inorg Chem* **2010**, *49*, 10283–10290.
- [23] a) K. Banlusan, E. Antillon, A. Strachan, *J Phys Chem C* **2015**, *119*, 25845–25852; b) D. F. Bahr, J. A. Reid, W. M. Mook, C. A. Bauer, R. Stumpf, A. J. Skulan, N. R. Moody, B. A. Simmons, M. M. Shindel, M. D. Allendorf, *Phys Rev B* **2007**, *76*, 184106; c) M. Mattesini, J. M. Soler, F. Yndurain, *Phys Rev B* **2006**, *73*, 094111.
- [24] S. Bordiga, C. Lamberti, G. Ricchiardi, L. Regli, F. Bonino, A. Damin, K. P. Lillerud, M. Bjorgen, A. Zecchina, *Chem Commun* **2004**, 2300–2301.
- [25] N. A. Rodriguez, R. Parra, M. A. Grela, *Rsc Adv* **2015**, *5*, 73112–73118.
- [26] C. G. Silva, A. Corma, H. Garcia, *J Mater Chem* **2010**, *20*, 3141–3156.
- [27] R. Diaz, M. G. Orcajo, J. A. Botas, G. Calleja, J. Palma, *Mater Lett* **2012**, *68*, 126–128.
- [28] I. A. Khan, Y. H. Qian, A. Badshah, M. A. Nadeem, D. Zhao, *Acs Appl Mater Inter* **2016**, *8*, 17268–17275.
- [29] A. J. Graham, D. R. Allan, A. Muszkiewicz, C. A. Morrison, S. A. Moggach, *Angew Chem Int Edit* **2011**, *50*, 11138–11141 (*Angew Chem* **2011**, *123*, 11334–11337).
- [30] L. H. He, F. Liu, G. Hautier, M. J. T. Oliveira, M. A. L. Marques, F. D. Vila, J. J. Rehr, G. M. Rignanese, A. H. Zhou, *Phys Rev B* **2014**, *89*, 064305.
- [31] a) H. Khajavi, J. Gascon, J. M. Schins, L. D. A. Siebbeles, F. Kapteijn, *J Phys Chem C* **2011**, *115*, 12487–12493; b) J. Gascon, M. D. Hernandez-Alonso, A. R. Almeida, G. P. M. van Klink, F. Kapteijn, G. Mul, *ChemSuschem* **2008**, *1*, 981–983.
- [32] D. Bagayoko, *Aip Adv* **2014**, *4*, 127104.
- [33] a) K. B. Wiberg, P. R. Rablen, *J Comput Chem* **1993**, *14*, 1504–1518; b) F. De Proft, C. Van Alsenoy, A. Peeters, W. Langenaeker, P. Geerlings, *J Comput Chem* **2002**, *23*, 1198–1209; c) W. Tang, E. Sanville, G. Henkelman, *J Phys-Condens Mat* **2009**, *21*, 084204.
- [34] a) M. Wu, H. B. Lou, J. S. Tse, H. Y. Liu, Y. M. Pan, K. Takahama, T. Matsuoka, K. Shimizu, J. H. Jiang, *Phys Rev B* **2016**, *94*, 054201; b) M. Wu, J. S. Tse, S. Y. Wang, C. Z. Wang, J. Z. Jiang, *Nat Commun* **2015**, *6*, 6493.

Submitted: May 8, 2018

Accepted: July 11, 2018